Conference Proceedings of the Society for Experimental Mechanics Series

Matt Allen · Randy Mayes · Daniel Rixen *Editors*

Dynamics of Coupled Structures, Volume 1

Proceedings of the 32nd IMAC, A Conference and Exposition on Structural Dynamics, 2014

SEM

Springer

Conference Proceedings of the Society for Experimental Mechanics Series

Series Editor
Tom Proulx
Society for Experimental Mechanics, Inc.,
Bethel, CT, USA

For further volumes:
http://www.springer.com/series/8922

Matt Allen • Randy Mayes • Daniel Rixen
Editors

Dynamics of Coupled Structures, Volume 1

Proceedings of the 32nd IMAC, A Conference and Exposition on Structural Dynamics, 2014

Springer

Editors
Matt Allen
Engineering Physics Department
University of Wisconsin Madison
Madison, WI, USA

Daniel Rixen
Lehrstuhl fur Angewandte Mechanik
Technische Universitat Munchen
Garching, Germany

Randy Mayes
Sandia National Laboratories
Albuquerque, NM, USA

ISSN 2191-5644 ISSN 2191-5652 (electronic)
ISBN 978-3-319-04500-9 ISBN 978-3-319-04501-6 (eBook)
DOI 10.1007/978-3-319-04501-6
Springer Cham Heidelberg New York Dordrecht London

Library of Congress Control Number: 2014932412

Printed on acid-free paper

Springer is part of Springer Science+Business Media (www.springer.com)

Preface

Dynamics of Coupled Structures, Volume 1 represents one of the eight volumes of technical papers presented at the 32nd IMAC, A Conference and Exposition on Structural Dynamics, 2014, organized by the Society for Experimental Mechanics, and held in Orlando, Florida, February 3–6, 2014. The full proceedings also include volumes on Nonlinear Dynamics; Model Validation and Uncertainty Quantification; Dynamics of Civil Structures; Structural Health Monitoring; Special Topics in Structural Dynamics; Topics in Modal Analysis I; and Topics in Modal Analysis II.

Each collection presents early findings from experimental and computational investigations on an important area within structural dynamics. Coupled structures, or substructuring, is one of these areas.

Substructuring is a general paradigm in engineering dynamics where a complicated system is analyzed by considering the dynamic interactions between subcomponents. In numerical simulations, substructuring allows one to reduce the complexity of parts of the system in order to construct a computationally efficient model of the assembled system. A subcomponent model can also be derived experimentally, allowing one to predict the dynamic behavior of an assembly by combining experimentally and/or analytically derived models. This can be advantageous for subcomponents that are expensive or difficult to model analytically. Substructuring can also be used to couple numerical simulation with real-time testing of components. Such approaches are known as hardware-in-the-loop or hybrid testing.

Whether experimental or numerical, all substructuring approaches have a common basis, namely the equilibrium of the substructures under the action of the applied and interface forces and the compatibility of displacements at the interfaces of the subcomponents. Experimental substructuring requires special care in the way the measurements are obtained and processed in order to assure that measurement inaccuracies and noise do not invalidate the results. In numerical approaches, the fundamental quest is the efficient computation of reduced order models describing the substructure's dynamic motion. For hardware-in-the-loop applications difficulties include the fast computation of the numerical components and the proper sensing and actuation of the hardware component. Recent advances in experimental techniques, sensor/actuator technologies, novel numerical methods, and parallel computing have rekindled interest in substructuring in recent years leading to new insights and improved experimental and analytical techniques.

The organizers would like to thank the authors, presenters, session organizers, and session chairs for their participation in this track.

Madison, WI, USA — M. Allen
Albuquerque, NM, USA — R. Mayes
Garching, Germany — D. Rixen

Contents

Chapter 1
Experimental-Analytical Dynamic Substructuring of Ampair Testbed: A State-Space Approach

Mladen Gibanica, Anders T. Johansson, Anders Liljerehn, Per Sjövall, and Thomas Abrahamsson

Abstract The Society for Experimental Mechanics (SEM) Substructuring Focus Group has initiated a research project in experimental dynamic substructuring using the Ampair 600W wind turbine as a testbed. In this paper, experimental as well as analytical models of the blades of said wind turbine are coupled to analytical models of its brackets. The focus is on a state-space based substructuring method designed specifically for experimental-analytical dynamic substructuring. It is shown (a) theoretically that the state-space method gives equivalent results to the second order methods under certain conditions, (b) that the state-space method numerically produces results equivalent to those of a well-known frequency-based substructuring technique when the same experimental models are used for the two methods and (c) that the state-space synthesis procedure can be translated to the general framework given by De Klerk et al.

Keywords Substructuring • Experimental-analytical dynamic • Modal analysis • Vibration testing • State-space • Component mode synthesis • Frequency based substructuring • Automatic system identification • Wind turbines

1.1 Introduction

The subject of substructuring has been an open research area ever since its advent in the 1960s [1]. Recently, often attributed to advances in computing capacity and experimental equipment, there has been a renewed interest in the subject. Substructuring builds on the idea that a complex structure can be decomposed into a number of simpler components, or substructures. The modeling approach of these substructures may vary, which allows creating mixed experimental and analytical models thereby increasing the modeling flexibility for complex mechanical structures such as cars, air planes, rocket launchers and wind turbines.

Although the main concept of substructuring is simple—a matter of enforcing compatibility and equilibrium at the interfaces between substructures—there are a number of different methods presented in literature. These are typically categorized, by the type of substructure models used, as Frequency Response Function (FRF) based and modal based (CMS—component mode synthesis) methods. Early works falling in the former category are e.g. [2, 3] while the Craig-Bampton method [4] is a well-known early representative of the latter. The paper by de Klerk et al. [1] is frequently cited as a well written overview of the field. This paper is based on the MSc thesis by Mr. Mladen Gibanica [5].

The structure under investigation here is the SEM Substructuring Focus Group testbed, the Ampair 600 wind turbine, further detailed by Mayes [6]. Since its introduction at IMAC XXX, several attempts at substructuring have been reported for this structure. A group from Sandia National Laboratories have worked with experimental substructuring using the Transmission Simulator Technique [7, 8], a method also employed at the Atomic Weapons Establishment in the UK [9],

M. Gibanica • A.T. Johansson (✉) • T. Abrahamsson
Department of Applied Mechanics, Chalmers University of Technology, SE-412 96 Göteborg, Sweden
e-mail: anders.t.johansson@chalmers.se

A. Liljerehn
AB Sandvik Coromant, R & D Metal Cutting Research, SE-811 81 Sandviken, Sweden

P. Sjövall
FS Dynamics, SE-412 63 Göteborg, Sweden

M. Allen et al. (eds.), *Dynamics of Coupled Structures, Volume 1: Proceedings of the 32nd IMAC, A Conference and Exposition on Structural Dynamics, 2014*, Conference Proceedings of the Society for Experimental Mechanics Series,
DOI 10.1007/978-3-319-04501-6_1,

while a frequency-based method was used by a group from TU Delft [10]. Also, a group of Italian scientists have studied the role of interface degrees of freedom for the coupling of the structure [11].

The purpose of the test bed is to serve as a reference for researchers around the world. Data is shared online through a wiki [12]. This paper considers the blades and the brackets of the turbine only—the hub, tower and base are thus left for later studies. The dynamics of the joints has not been considered (a presentation on nonlinear effects from varying contact geometry at different load levels was given by Dr. Pascal Reuss at IMAC XXXI [13]). Components are coupled using the state-space synthesis method of [14]. (Similar methods have been proposed also by e.g. Su and Juang [15].) The results are compared to experimental measurements of the assembly as well as experimental-analytical FRF-based coupling techniques and analytical models coupled using CMS. The Ampair 600 wind turbine blades, consisting of a composite hull around a solid core, have been thoroughly tested in dynamic and static measurements as well as destructive tests to quantify the material parameters [16–21]. A calibrated FE model of the blades has been developed by Johansson et al. [20] which is used for comparison here. A new FE model of the bracket is created from geometry measurements made available by the TU Delft and using standard material properties.

The paper is structured as follows: Sect. 1.2 briefly introduces the theory behind the state space coupling technique and puts it into the framework of de Klerk et al. [1]. Section 1.3 describes the Finite Element models used. Section 1.4 elaborates on performed experiments and describes the experimentally derived models used. Section 1.5 relates results before the paper is rounded up by some conclusions in Sect. 1.6.

1.2 Theory

In linear system theory, systems are sometimes separated into *external* and *internal* descriptions, where the former offer information on the input-output relation only whereas the latter includes information on the *state* of the process [22, 23]. The typical external model in structural dynamics is the time domain convolution relation which gives rise to the Frequency Response Function in the frequency domain:

$$\mathbf{y}(t) = \mathbf{y}_0 + \int_0^{\infty} \mathbf{h}(t-\tau)\mathbf{u}(\tau)d\tau \tag{1.1}$$

$$\mathbf{Y}(\omega) = \mathbf{H}(\omega)\mathbf{U}(\omega) \tag{1.2}$$

While internal models are given in the usual first- or second-order forms [24]:

$$\begin{cases} \dot{\mathbf{x}}(t) = \mathbf{A}\mathbf{x}(t) + \mathbf{B}\mathbf{u}(t) \\ \mathbf{y}(t) = \mathbf{C}\mathbf{x}(t) + \mathbf{D}\mathbf{u}(t) \end{cases} \tag{1.3}$$

$$\mathbf{K}\mathbf{q}(t) + \mathbf{V}\dot{\mathbf{q}}(t) + \mathbf{M}\ddot{\mathbf{q}}(t) = \mathbf{f}(t) \tag{1.4}$$

where the matrices have the usual meanings and the forces in Eq. (1.4) relate to the input in Eq. (1.3) through a selection matrix such that $\mathbf{f}(t) = \mathbf{P}_u\mathbf{u}(t)$ [25]. A shaker or impact hammer testing campaign will thus result in an external model of the system, from which the analyst frequently attempts to derive an internal model. This process is often referred to as *modal parameter extraction* [26] in the structural dynamics community and *system identification* elsewhere [27].

1.2.1 System Identification

System identification is performed on experimentally obtained outer models in the frequency domain, Eq. (1.2), using the state-space subspace system identification algorithm implemented as `n4sid` in MATLAB's System Identification Toolbox [27, 28] to estimate a state-space model quadruple set $\{\mathbf{A}, \mathbf{B}, \mathbf{C}, \mathbf{D}\}$. In order to automate the system identification process a method for automatic model order estimation by Yaghoubi and Abrahamsson [29] is used along with the N4SID method.

All systems studied in this paper are considered to be linear time invariant (LTI) systems. By assumption they are also stable and passive. The systems are also assumed to be reciprocal (since the systems are non-gyroscopic and non-circulatory). As system identification is a general tool, these assumptions must be enforced explicitly (except for stability, which can be included as a condition on the system identification algorithm). Reciprocity is enforced through measuring using a limited number of input nodes and applying Maxwell-Betti's reciprocity principle (see [5]). The passivity criterion states that the power supplied to the system is non-negative and can be zero only for components without damping. Models derived from first principles satisfy the passivity criterion implicitly, but this is not necessarily the case for experimentally identified models. The passivity problem for state space models is commonly known, for details see for example [14, 30]. The passivity of a state space model is linked to the positive real (PR) lemma. In this paper, an engineering solution to the passivity optimization problem defined in [14] based on averaging of the **B** and **C** matrices has been used.

1.2.2 Substructuring

Substructuring is the process of coupling two structures together by enforcing two conditions at their common interface; compatibility and force equilibrium. This paper will treat only what de Klerk et al. [1] refers to as the primal formulation, which implies that the displacements are defined and interface forces are eliminated. For brevity, the explicit time dependency is dropped from the equations in the following.

For (analytically derived) internal models as in Eq. (1.4), enforcing compatibility and force equilibrium amounts to an assembly procedure parallel to that used for Finite Element Models, see further de Klerk et al. [1], such that synthesis of two systems 1 and 2 can be described by:

$$\begin{cases} \begin{bmatrix} \mathbf{K}_1 & \mathbf{0} \\ \mathbf{0} & \mathbf{K}_2 \end{bmatrix} \begin{Bmatrix} \mathbf{q}_1 \\ \mathbf{q}_2 \end{Bmatrix} + \begin{bmatrix} \mathbf{V}_1 & \mathbf{0} \\ \mathbf{0} & \mathbf{V}_2 \end{bmatrix} \begin{Bmatrix} \dot{\mathbf{q}}_1 \\ \dot{\mathbf{q}}_2 \end{Bmatrix} + \begin{bmatrix} \mathbf{M}_1 & \mathbf{0} \\ \mathbf{0} & \mathbf{M}_2 \end{bmatrix} \begin{Bmatrix} \ddot{\mathbf{q}}_1 \\ \ddot{\mathbf{q}}_2 \end{Bmatrix} = \mathbf{f} + \mathbf{g} \\ \mathbf{E}\mathbf{q} = \mathbf{0} \\ \mathbf{L}^T\mathbf{g} = \mathbf{0} \end{cases} \tag{1.5}$$

where **E** can be thought of as a signed boolean matrix enforcing compatibility,[1] **g** are the interface forces, and the matrix **L** is the nullspace of **E**. For details, refer to [1]. When coupling two structures, which are described by m_1 and m_2 degrees of freedom (DOFs), the assembled structure will consist of $m_1 + m_2 - m_c$ coordinates, where m_c is the number of coupling constraints. The de Klerk et al. paper [1] generalizes the formulation using the two matrices **E** and **L** to include also models using generalized coordinates and outer models (Eq. (1.2)), i.e. FRF coupling. In a following subsection, the state-space method [14] will be put into the same format.

1.2.3 State-Space Coupling

The state-space coupling used here is described in the paper by Sjövall and Abrahamsson [14]. At its core is the *coupling form* of Eq. (1.6), where the i:th first-order system to be coupled is rewritten to second-order form at the interface in order for the compatibility and force equilibrium conditions to be applicable

$$\begin{cases} \begin{bmatrix} \ddot{\mathbf{y}}_c \\ \dot{\mathbf{y}}_c \\ \dot{\mathbf{x}}_b \end{bmatrix} = \begin{bmatrix} \mathbf{A}^i_{vv} & \mathbf{A}^i_{vd} & \mathbf{A}^i_{vb} \\ \mathbf{I} & \mathbf{0} & \mathbf{0} \\ \mathbf{0} & \mathbf{A}^i_{bd} & \mathbf{A}^i_{bb} \end{bmatrix} \begin{bmatrix} \dot{\mathbf{y}}_c \\ \mathbf{y}_c \\ \mathbf{x}_b \end{bmatrix} + \begin{bmatrix} \mathbf{B}^i_{vv} & \mathbf{B}^i_{vb} \\ \mathbf{0} & \mathbf{0} \\ \mathbf{0} & \mathbf{B}^i_{bb} \end{bmatrix} \begin{bmatrix} \mathbf{u}_c \\ \mathbf{u}_d \end{bmatrix} \\ \begin{bmatrix} \mathbf{y}_c \\ \mathbf{y}_d \end{bmatrix} = \begin{bmatrix} \mathbf{0} & \mathbf{I} & \mathbf{0} \\ \mathbf{C}^i_{bv} & \mathbf{C}^i_{bd} & \mathbf{C}^i_{bb} \end{bmatrix} \end{cases} \tag{1.6}$$

Here, the subscript c refers to coupling degrees of freedom, b other degrees of freedom, v velocity outputs and d displacement outputs. Note that for state-space coupling there exist twice as many states as DOFs (a product of rewriting a second-order differential equation on first-order form) and thus if $n = 2m$, for two structures with n_1 and n_2 states and m_c coupling coordinates the coupled system will contain $n_1 + n_2 - 2m_c$ states.

---

[1] This matrix is denoted **B** in de Klerk et al. The notation cannot be adopted here as the **B** matrix is strongly associated to the state-space formulation in Eq. (1.3).

1.2.3.1 General Framework

Here, the coupling procedure derived in [14] is recast into the general framework established by de Klerk et al. [1], thus using the $\mathbf{E}$ and $\mathbf{L}$ matrices defined above.

Starting from a general state-space formulation (Eq. (1.3)), a transformation matrix $\mathbf{T}$ is introduced which takes the system to the coupling form of Eq. (1.6) [14]. Let the system on coupling form be:

$$\begin{cases} \dot{\tilde{\mathbf{x}}} = \tilde{\mathbf{A}}\tilde{\mathbf{x}} + \tilde{\mathbf{B}}\mathbf{u} \\ \mathbf{y} = \tilde{\mathbf{C}}\tilde{\mathbf{x}} \end{cases} \tag{1.7}$$

where $\tilde{\mathbf{A}} = \mathbf{T}^{-1}\mathbf{A}\mathbf{T}$, $\tilde{\mathbf{B}} = \mathbf{T}\mathbf{B}$, $\tilde{\mathbf{C}} = \mathbf{C}\mathbf{T}^{-1}$ and $\tilde{\mathbf{x}} = \mathbf{T}\mathbf{x}$. $\mathbf{B}_{vv}$ of Eq. (1.6) is the inertia at the interface DOFs [31]. By forming of a new matrix denoted $\mathbf{M}_B$, the system can be rewritten such that the first block row is pre-multiplied by $\mathbf{B}_{vv}^{-1}$. The matrix $\mathbf{M}_B$ will then be:

$$\mathbf{M}_B = diag(diag(\mathbf{B}_{vv}^{1^{-1}}, \mathbf{I}, \mathbf{I}), \ldots, diag(\mathbf{B}_{vv}^{h^{-1}}, \mathbf{I}, \mathbf{I})) \tag{1.8}$$

Such that the system can now be written as:

$$\begin{cases} \mathbf{M}_B\dot{\tilde{\mathbf{x}}} = \mathbf{M}_B\tilde{\mathbf{A}}\tilde{\mathbf{x}} + \mathbf{M}_B\tilde{\mathbf{B}}\mathbf{u} \\ \mathbf{y} = \tilde{\mathbf{C}}\tilde{\mathbf{x}} \end{cases} \tag{1.9}$$

Introducing the $\mathbf{E}$ and $\mathbf{L}$ matrices such that compatibility is described by $\mathbf{E}\tilde{\mathbf{x}} = \mathbf{0}$ and equilibrium by $\mathbf{L}^T\mathbf{u}_{c,g} = \mathbf{0}$, where subscript g is used to denote interface forces, the matrix $\mathbf{L}$ is formed as $\mathbf{L} = null(\mathbf{E})$ such that the following is satisfied: $\mathbf{E}\tilde{\mathbf{x}} = \mathbf{E}\mathbf{L}\tilde{\mathbf{z}} = \mathbf{0}$ and $\tilde{\mathbf{x}} = \mathbf{L}\tilde{\mathbf{z}}$. The new state vector $\tilde{\mathbf{z}}$ represents the new states after coupling. The synthesised state-space model is then formed as follows:

$$\begin{cases} \mathbf{L}^T\mathbf{M}_B\mathbf{L}\dot{\tilde{\mathbf{z}}} = \mathbf{L}^T\mathbf{M}_B\tilde{\mathbf{A}}\mathbf{L}\tilde{\mathbf{z}} + \mathbf{L}^T\mathbf{M}_B\tilde{\mathbf{B}}\mathbf{u} \\ \mathbf{y} = \tilde{\mathbf{C}}\mathbf{L}\tilde{\mathbf{z}} \end{cases} \tag{1.10}$$

Finally, $(\mathbf{L}^T\mathbf{M}_B\mathbf{L})^{-1}$, may be pre-multiplied to the first equation in Eq. (1.10). A new transformation matrix must however be introduced simply to reduce the excess inputs and outputs. The new matrix is denoted $\mathbf{L}_u$ and is formed from a matrix $\mathbf{E}_u$ as before, $\mathbf{L}_u = null(\mathbf{E}_u)$. In other words, for a system with two synthesised components the new reduction matrix is $\mathbf{E}_u = [\mathbf{I} \quad \mathbf{0} \quad \mathbf{0} \quad \mathbf{0}]$. The implication of this transformation is that in the synthesised model, to which this new matrix is applied, the first component of the considered vector will be removed. This new matrix is introduced in the equations by the transformations $\mathbf{u} = \mathbf{L}_u\bar{\mathbf{u}}$ and $\bar{\mathbf{y}} = \mathbf{L}_u^T\mathbf{y}$ as shown in Eq. (1.12). The last step is only true for systems with an equal number of inputs and outputs but is easily generalised. The final system can be written as follows:

$$\begin{cases} \dot{\tilde{\mathbf{z}}} = \hat{\mathbf{A}}\tilde{\mathbf{z}} + \hat{\mathbf{B}}\bar{\mathbf{u}} \\ \bar{\mathbf{y}} = \hat{\mathbf{C}}\tilde{\mathbf{z}} \end{cases} \tag{1.11}$$

Where each part in the equation above is then identified as:

$$\begin{cases} \hat{\mathbf{A}} = (\mathbf{L}^T\mathbf{M}_B\mathbf{L})^{-1}(\mathbf{L}^T\mathbf{M}_B\tilde{\mathbf{A}}\mathbf{L}) \\ \hat{\mathbf{B}} = (\mathbf{L}^T\mathbf{M}_B\mathbf{L})^{-1}(\mathbf{L}^T\mathbf{M}_B\tilde{\mathbf{B}})\mathbf{L}_u \\ \hat{\mathbf{C}} = \mathbf{L}_u^T(\tilde{\mathbf{C}}\mathbf{L}) \end{cases} \tag{1.12}$$

1.2.3.2 Second Order Form Equivalent of Synthesised First Order Form

An analytical model written on second order form can easily be rewritten on first order form by doubling the number of states [24]. The transformation from a first order form to a second order form with half the number of states is not as trivial, even when possible.

Begin the second order system shown in Eq. (1.5). Methods for rewriting such a system to the first-order form of Eq. (1.3) are well-known [24, 25]. It is assumed that the output is the entire displacement vector, such that all DOFs are considered as outputs. A transformation matrix is introduced in Eq. (1.13) which transforms a state-space system to coupling form under the assumption that the original system is analytically derived with state vector $\mathbf{x}^T = \begin{bmatrix}\mathbf{q}\ \dot{\mathbf{q}}\end{bmatrix}^T$ and displacement output such that $\mathbf{q} = \mathbf{y} = \mathbf{C}\mathbf{x}$

$$\mathbf{T}^i = \begin{bmatrix} \mathbf{C}_c^i \mathbf{A}^i \\ \mathbf{C}_c^i \\ \mathbf{C}_b^i \mathbf{A}^i \\ \mathbf{C}_b^i \end{bmatrix} \tag{1.13}$$

This transformation will produce a new state vector, $\tilde{\mathbf{x}} = \begin{bmatrix}\dot{\mathbf{y}}_c^i\ \mathbf{y}_c^i\ \dot{\mathbf{y}}_b^i\ \mathbf{y}_b\end{bmatrix}^T$, where the superscript i represents the subcomponent system. Again, the subscript c denotes the coupling partition of the input and output matrices, i.e. the block row and column of the $\mathbf{B}$ and $\mathbf{C}$ matrices, respectively. The difference between this transformation and the transformation in [14], is that the internal states are represented by physical coordinates here. In a theoretical representation this is valid, but in an experimental representation it would imply a significant constraint on the model to allow only twice as many states as there are sensors. The coupling form obtained through Eq. (1.13) is shown below

$$\begin{cases} \tilde{\mathbf{A}}^i = \mathbf{T}^i \mathbf{A}^i \mathbf{T}^{i^{-1}} = \begin{bmatrix} \mathbf{A}_{cvc}^i & \mathbf{A}_{cdc}^i & \mathbf{A}_{cvb}^i & \mathbf{A}_{cdb}^i \\ \mathbf{I} & \mathbf{0} & \mathbf{0} & \mathbf{0} \\ \mathbf{A}_{bvc}^i & \mathbf{A}_{bdc}^i & \mathbf{A}_{bvb}^i & \mathbf{A}_{bdb}^i \\ \mathbf{0} & \mathbf{0} & \mathbf{I} & \mathbf{0} \end{bmatrix} \\ \tilde{\mathbf{B}}^i = \mathbf{T}^i \mathbf{B}^i = \begin{bmatrix} \mathbf{C}_c^i \mathbf{A}^i \mathbf{B}^i \\ \mathbf{C}_c^i \mathbf{B}^i \\ \mathbf{C}_b^i \mathbf{A}^i \mathbf{B}^i \\ \mathbf{C}_b^i \mathbf{B}^i \end{bmatrix} = \begin{bmatrix} \mathbf{C}_c^i \mathbf{A}^i \mathbf{B}^i \\ \mathbf{0} \\ \mathbf{C}_b^i \mathbf{A}^i \mathbf{B}^i \\ \mathbf{0} \end{bmatrix} = \begin{bmatrix} \mathbf{B}_{c,c}^i & \mathbf{B}_{c,b}^i \\ \mathbf{0} & \mathbf{0} \\ \mathbf{B}_{bc}^i & \mathbf{B}_{bb}^i \\ \mathbf{0} & \mathbf{0} \end{bmatrix} \\ \tilde{\mathbf{C}}^i = \mathbf{C}^i \mathbf{T}^{i^{-1}} = \begin{bmatrix} \mathbf{I}\ \mathbf{0}\ \mathbf{0}\ \mathbf{0} \\ \mathbf{0}\ \mathbf{0}\ \mathbf{I}\ \mathbf{0} \end{bmatrix} \end{cases} \tag{1.14}$$

It can be shown that the transformation of the input matrix $\mathbf{CAB}$, with the assumptions introduced above, is but the inverse of the mass matrix, thus simplifying the $\tilde{\mathbf{B}}$ matrix as follows (recall that the full system mass matrix is a block-diagonal matrix):

$$\begin{cases} \mathbf{B}_{cc}^i = \mathbf{M}_{cc}^{i^{-1}} \\ \mathbf{B}_{cb}^i = \mathbf{0} \\ \mathbf{B}_{bc}^i = \mathbf{0} \\ \mathbf{B}_{bb}^i = \mathbf{M}_{bb}^{i^{-1}} \end{cases} \tag{1.15}$$

Synthesising two systems by the procedure described above yields the following model, here reorganised such that it is recognisable as the usual state-space formulation of a second order system [25]:

$$\begin{gathered} \begin{Bmatrix} \dot{\bar{\mathbf{y}}}_c \\ \dot{\mathbf{y}}_b^1 \\ \dot{\mathbf{y}}_b^2 \\ \ddot{\bar{\mathbf{y}}}_c \\ \ddot{\mathbf{y}}_b^1 \\ \ddot{\mathbf{y}}_b^2 \end{Bmatrix} = \begin{bmatrix} \mathbf{0} & \mathbf{0} & \mathbf{0} & \mathbf{I} & \mathbf{0} & \mathbf{0} \\ \mathbf{0} & \mathbf{0} & \mathbf{0} & \mathbf{0} & \mathbf{I} & \mathbf{0} \\ \mathbf{0} & \mathbf{0} & \mathbf{0} & \mathbf{0} & \mathbf{0} & \mathbf{I} \\ \bar{\mathbf{A}}_{cdc} & \bar{\mathbf{A}}_{cdb}^1 & \bar{\mathbf{A}}_{cdb}^2 & \bar{\mathbf{A}}_{cvc} & \bar{\mathbf{A}}_{cvb}^1 & \bar{\mathbf{A}}_{cvb}^2 \\ \mathbf{A}_{bdc}^1 & \mathbf{A}_{bdb}^1 & \mathbf{0} & \mathbf{A}_{bvc}^1 & \mathbf{A}_{bvb}^1 & \mathbf{0} \\ \mathbf{A}_{bdc}^2 & \mathbf{0} & \mathbf{A}_{bdb}^2 & \mathbf{A}_{bvc}^2 & \mathbf{0} & \mathbf{A}_{bvb}^2 \end{bmatrix} \begin{Bmatrix} \bar{\mathbf{y}}_c \\ \mathbf{y}_b^1 \\ \mathbf{y}_b^2 \\ \dot{\bar{\mathbf{y}}}_c \\ \dot{\mathbf{y}}_b^1 \\ \dot{\mathbf{y}}_b^2 \end{Bmatrix} + \begin{bmatrix} \mathbf{0} & \mathbf{0} & \mathbf{0} \\ \mathbf{0} & \mathbf{0} & \mathbf{0} \\ \mathbf{0} & \mathbf{0} & \mathbf{0} \\ \bar{\mathbf{B}}_{cc} & \mathbf{0} & \mathbf{0} \\ \mathbf{0} & \mathbf{B}_{bb}^1 & \mathbf{0} \\ \mathbf{0} & \mathbf{0} & \mathbf{B}_{bb}^2 \end{bmatrix} \begin{Bmatrix} \bar{\mathbf{u}}_c \\ \mathbf{u}_b^1 \\ \mathbf{u}_b^2 \end{Bmatrix} \\ \begin{Bmatrix} \bar{\mathbf{y}}_c \\ \mathbf{y}_b^1 \\ \mathbf{y}_b^2 \end{Bmatrix} = \begin{bmatrix} \mathbf{I}\ \mathbf{0}\ \mathbf{0}\ \mathbf{0}\ \mathbf{0}\ \mathbf{0} \\ \mathbf{0}\ \mathbf{I}\ \mathbf{0}\ \mathbf{0}\ \mathbf{0}\ \mathbf{0} \\ \mathbf{0}\ \mathbf{0}\ \mathbf{I}\ \mathbf{0}\ \mathbf{0}\ \mathbf{0} \end{bmatrix} \begin{Bmatrix} \bar{\mathbf{y}}_c \\ \mathbf{y}_b^1 \\ \mathbf{y}_b^2 \\ \dot{\bar{\mathbf{y}}}_c \\ \dot{\mathbf{y}}_b^1 \\ \dot{\mathbf{y}}_b^2 \end{Bmatrix} \end{gathered} \tag{1.16}$$

The lower part can be identified as a second order system which is directly comparable to the direct coupling procedure [1]. The two second order systems can be written with an interface part (c) and a body part (b) for two components, $i = 1, 2$.

$$
\begin{cases}
\mathbf{M}^i = \begin{bmatrix} \mathbf{M}^i_{cc} & \mathbf{0} \\ \mathbf{0} & \mathbf{M}^i_{bb} \end{bmatrix} \\
\mathbf{K}^i = \begin{bmatrix} \mathbf{K}^i_{cc} & \mathbf{K}^i_{cb} \\ \mathbf{K}^i_{bc} & \mathbf{K}^i_{bb} \end{bmatrix} \\
\mathbf{V}^i = \begin{bmatrix} \mathbf{V}^i_{cc} & \mathbf{V}^i_{cb} \\ \mathbf{V}^i_{bc} & \mathbf{V}^i_{cc} \end{bmatrix}
\end{cases}
\tag{1.17}
$$

The synthesised system then becomes

$$
\begin{cases}
\mathbf{M}_{as} = \begin{bmatrix} \mathbf{M}^1_{cc} + \mathbf{M}^2_{cc} & \mathbf{0} & \mathbf{0} \\ \mathbf{0} & \mathbf{M}^1_{bb} & \mathbf{0} \\ \mathbf{0} & \mathbf{0} & \mathbf{M}^2_{bb} \end{bmatrix} \\
\mathbf{K}_{as} = \begin{bmatrix} \mathbf{K}^1_{cc} + \mathbf{K}^2_{cc} & \mathbf{K}^1_{cb} & \mathbf{K}^2_{cb} \\ \mathbf{K}^1_{bc} & \mathbf{K}^1_{bb} & \mathbf{0} \\ \mathbf{K}^2_{bc} & \mathbf{0} & \mathbf{K}^2_{bb} \end{bmatrix} \\
\mathbf{V}_{as} = \begin{bmatrix} \mathbf{V}^1_{cc} + \mathbf{V}^2_{cc} & \mathbf{V}^1_{cb} & \mathbf{V}^2_{cb} \\ \mathbf{V}^1_{bc} & \mathbf{V}^1_{bb} & \mathbf{0} \\ \mathbf{V}^2_{bc} & \mathbf{0} & \mathbf{V}^2_{bb} \end{bmatrix}
\end{cases}
\tag{1.18}
$$

For comparison, the second order system from Eq. (1.16) is pre-multiplied by the inverse of its input matrix, which is diagonal. The resulting matrix is split in two, one part representing the stiffness and the other the damping. The following is then obtained

$$
\begin{cases}
\mathbf{M}_{as} \equiv \mathbf{M}_{sss} = \begin{bmatrix} \bar{\mathbf{B}}^{-1}_{cc} & \mathbf{0} & \mathbf{0} \\ \mathbf{0} & \bar{\mathbf{B}}^{1^{-1}}_{bb} & \mathbf{0} \\ \mathbf{0} & \mathbf{0} & \bar{\mathbf{B}}^{2^{-1}}_{bb} \end{bmatrix} = \begin{bmatrix} \mathbf{M}^1_{cc} + \mathbf{M}^2_{cc} & \mathbf{0} & \mathbf{0} \\ \mathbf{0} & \mathbf{M}^1_{bb} & \mathbf{0} \\ \mathbf{0} & \mathbf{0} & \mathbf{M}^2_{bb} \end{bmatrix} \\
\mathbf{K}_{as} \equiv \mathbf{K}_{sss} = \begin{bmatrix} \bar{\mathbf{B}}^{-1}_{cc}\bar{\mathbf{A}}_{cdc} & \bar{\mathbf{B}}^{-1}_{cc}\bar{\mathbf{A}}^1_{cdb} & \bar{\mathbf{B}}^{-1}_{cc}\bar{\mathbf{A}}^2_{cdb} \\ \bar{\mathbf{B}}^{1^{-1}}_{bb}\mathbf{A}^1_{bdc} & \bar{\mathbf{B}}^{1^{-1}}_{bb}\mathbf{A}^1_{bdb} & \mathbf{0} \\ \bar{\mathbf{B}}^{2^{-1}}_{bb}\mathbf{A}^2_{bdc} & \mathbf{0} & \bar{\mathbf{B}}^{2^{-1}}_{bb}\mathbf{A}^2_{bdb} \end{bmatrix} = \begin{bmatrix} \mathbf{K}^1_{cc} + \mathbf{K}^2_{cc} & \mathbf{K}^1_{cb} & \mathbf{K}^2_{cb} \\ \mathbf{K}^1_{bc} & \mathbf{K}^1_{bb} & \mathbf{0} \\ \mathbf{K}^2_{bc} & \mathbf{0} & \mathbf{K}^2_{bb} \end{bmatrix} \\
\mathbf{V}_{as} \equiv \mathbf{V}_{sss} = \begin{bmatrix} \bar{\mathbf{B}}^{-1}_{cc}\bar{\mathbf{A}}_{cvc} & \bar{\mathbf{B}}^{-1}_{cc}\bar{\mathbf{A}}^1_{cvb} & \bar{\mathbf{B}}^{-1}_{cc}\bar{\mathbf{A}}^2_{cvb} \\ \bar{\mathbf{B}}^{1^{-1}}_{bb}\mathbf{A}^1_{bvc} & \bar{\mathbf{B}}^{1^{-1}}_{bb}\mathbf{A}^1_{bvb} & \mathbf{0} \\ \bar{\mathbf{B}}^{2^{-1}}_{bb}\mathbf{A}^2_{bvc} & \mathbf{0} & \bar{\mathbf{B}}^{2^{-1}}_{bb}\mathbf{A}^2_{bvb} \end{bmatrix} = \begin{bmatrix} \mathbf{V}^1_{cc} + \mathbf{V}^2_{cc} & \mathbf{V}^1_{cb} & \mathbf{V}^2_{cb} \\ \mathbf{V}^1_{bc} & \mathbf{V}^1_{bb} & \mathbf{0} \\ \mathbf{V}^2_{bc} & \mathbf{0} & \mathbf{V}^2_{bb} \end{bmatrix}
\end{cases}
\tag{1.19}
$$

It is now obvious that both methods produce exactly the same systems.

1.3 Analytical Models

The two analytical FE models that were used were created in FEMAP and solved with MD Nastran. NX Nastran was used for verification where non-reduced models were solved.

1.3.1 Blade

A version of the blade FE model described in [20] (Nastran model can be found online at [12]) was used and is visualised in Fig. 1.1. The model consisted of 20,523 nodes and 96,416 elements. The model has a solid core, for which solid elements were used and a laminate skin model, for which laminate plate elements were used. For a thorough explanation of the composite material model and how it was calibrated, see Johansson et al. [20] (Fig. 1.2).

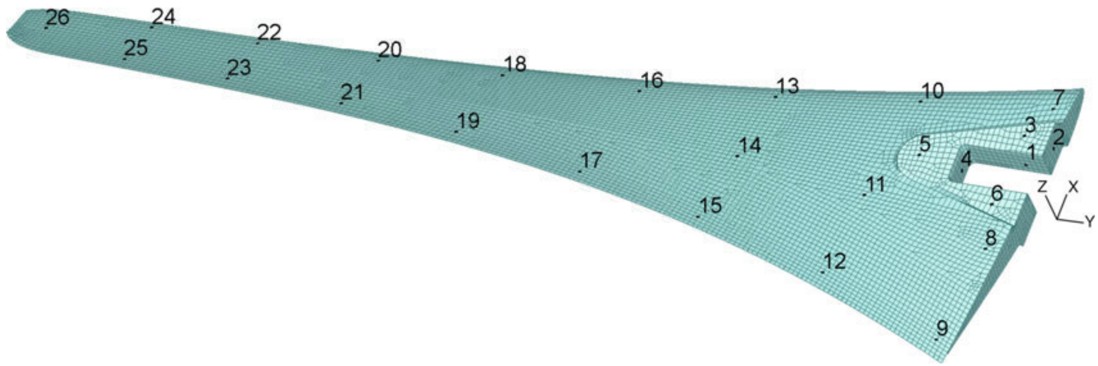

Fig. 1.1 FE model of the blade with numbering used in the FE model but also during the vibration tests

Fig. 1.2 Close-up view of the three inputs of the blade

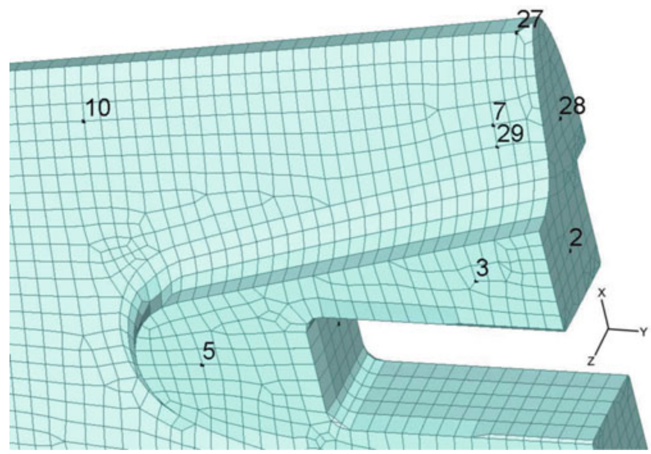

The accelerometer positions in the vibrations test and for the FE blade model are shown in Fig. 1.1. These were chosen as close to the physical locations of the accelerometers as possible for the MAC correlations to yield correct results. Note that the numbering starts at the coupling positions.

1.3.2 Bracket

The bracket geometry was received from TU Delft. It was modelled by 24,707 solid parabolic elements and an isotropic material model with stiffness $E = 2 \cdot 10^{11}$ N/m^2 and density $\rho = 5{,}000$ kg/m^3. The shaft which is inserted into the bracket was modelled as an integrated part of the bracket. Parabolic elements were used so that the shaft curvature would be described better. The bracket model is shown in Fig. 1.3. The numbers 1, 2 and 3 are the coupling positions coupled to the blade at positions 3, 4 and 5, thus matching DOFs were used at each of the components coupling locations.

1.3.3 FE Coupling

The coupling between the blade and the bracket can be seen in Fig. 1.4a, b, where the area around the holes on the blade have been constrained with rigid links. All the DOFs on the bracket in contact with the blade when mounted were constrained with rigid links to a six DOFs node located at the centre of the three holes. The bracket coupling type was constrained at the holes, see Fig. 1.4b. The same configurations were used in the experimental-analytical coupling. All three configurations were used in coupling of the analytical models. It should be noted that the blade bracket constraints configuration are on the same side of the blade which creates asymmetric modeshapes.

The assembled blade bracket structure along with the measurement points can be seen in Fig. 1.5.

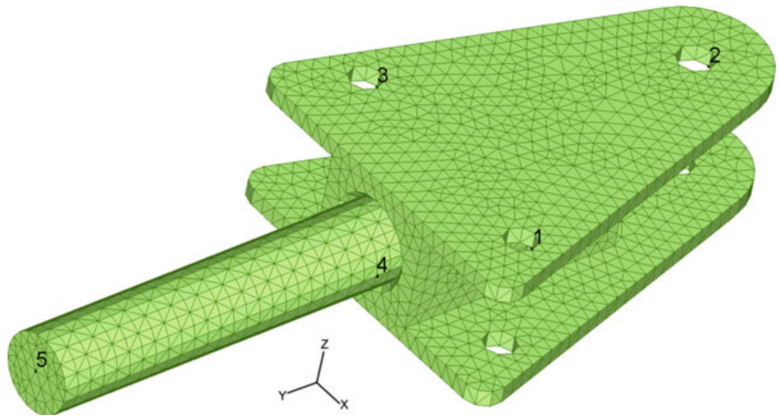

Fig. 1.3 FE model of the blade with numbering used in the FE model and during the vibration tests

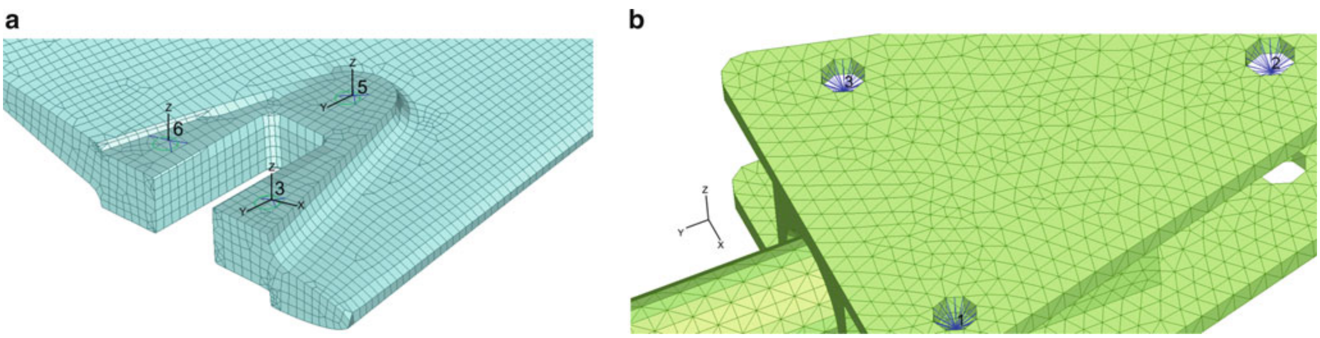

Fig. 1.4 The coupling configurations for the blade and the bracket using rigid links attached to a six DOFs coupling node. (**a**) Blade coupling configuration. (**b**) Bracket coupling configuration

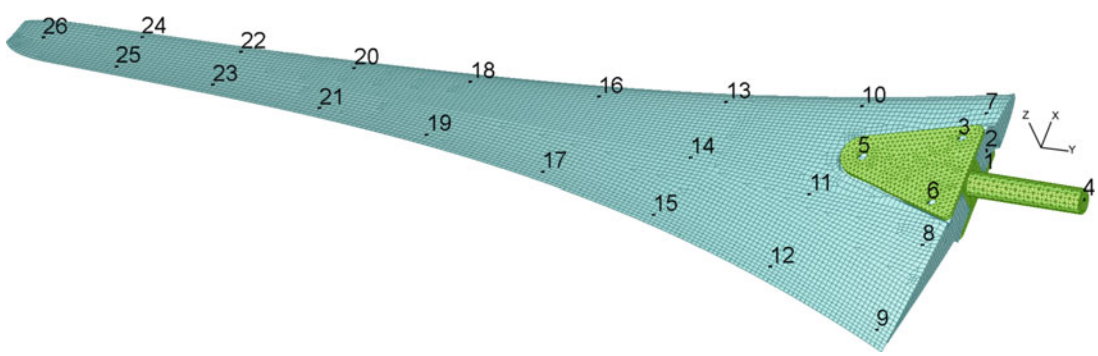

Fig. 1.5 The FE model of the blade mounted to the FE model of the bracket with measurement locations

1.4 Experiments

Three different blades from the same Ampair 600 wind turbine were considered. Each blade had a unique mounting brackets so that each blade was mounted to its own bracket. The three experimental blades will henceforth be denoted by their serial number; 841, 722 and 819 and the brackets will be numbered, 01, 02 and 03. Coupling between the blade and their corresponding bracket was blade 841 and bracket 01, blade 722 and bracket 02 and blade 819 and bracket 03. The bracket numbers will usually be omitted when the blade bracket configuration is discussed but occasionally they will be abbreviated as blade/bracket, e.g. 841/01 would represent a blade 841 which in turn is mounted to bracket 01.

The experiments were performed at Chalmers Vibration and Smart Structures Lab. The measurements were performed with a stepped sine input with 0.25 Hz step size from 20 to 800 Hz for the blade and blade bracket measurements. For the fully assembled system the measurements were performed from 10 to 300 Hz with a step size of 0.1 and 0.01 Hz at some particular frequency intervals. A total of three measurements for the blade and blade bracket models were made. The configurations

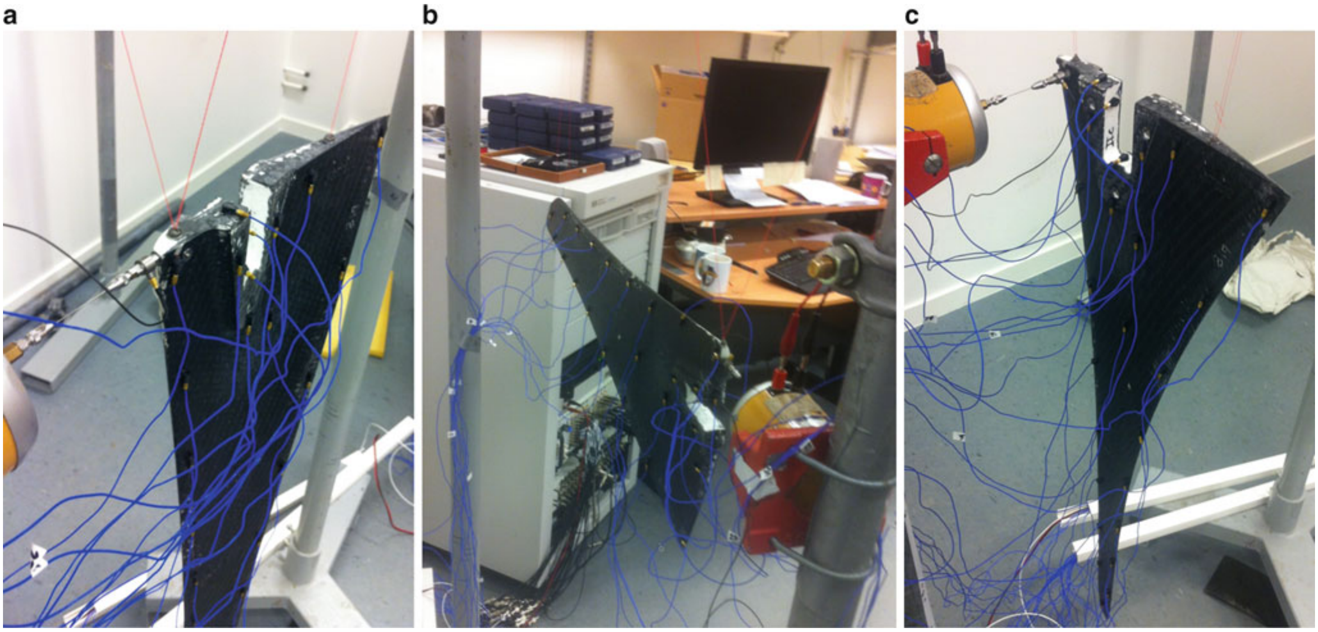

Fig. 1.6 The input directions and test setup for the blades. (**a**) Input in the x direction. (**b**) Input in the y direction. (**c**) Input in the z direction

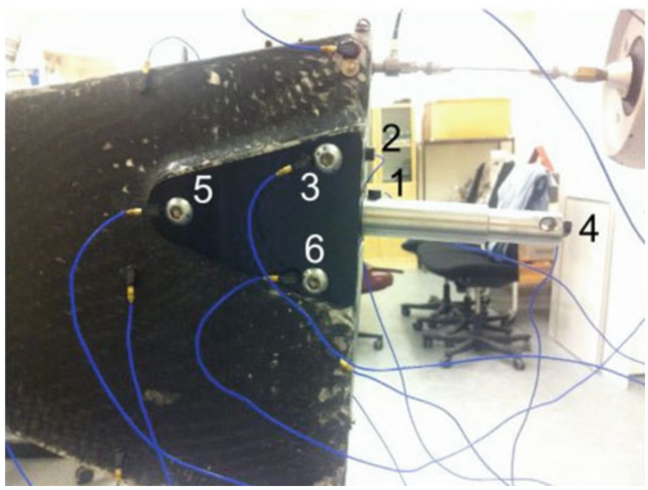

Fig. 1.7 A detailed view of the blade bracket assembly is shown with the accelerometer placements

considered were: the three blades alone and the three blades with brackets mounted. Note that measurements made in a specific direction (x, y or z) means that the input was aligned with that axis. See Fig. 1.1 for an orientation of an generic blade and Fig. 1.2 for the different input locations.

1.4.1 Test Setup

The three different input directions are shown in Fig. 1.6. This coordinate system is consistent with the FE analysis coordinate system. The test setup shown in Fig. 1.4 is also general for all measurements. It was exactly the same, both for the measurement of blades alone and for the blade measurements with a bracket attached. It can be seen, from Fig. 1.6, that the measured blades (and bracket mounted blades) were hung at three locations when measured in the x and y directions, which made it easier to position the components relative to the load cell. Measurements in the z direction for the blade and blade with attached bracket were only hung at two positions. Further, it should be noted that the components were hung in fasteners which were glued to the components, the same fastener was used for the load cell attachment and can be seen in Fig. 1.7. All the fasteners were mounted on the blades during all measurements for consistency.

The interface locations of the blade are shown in Fig. 1.2 but with the interface accelerometer from position 6 located under the stinger and used as a direct accelerance for a comparison with the accelerometer at position 1.

For a view of a bracket and blade assembled see Fig. 1.7. A detailed view of the interface accelerometers can also be seen. Different input directions to the bracket coupled with a blade had the same accelerometer locations and the same input locations were used as shown in Fig. 1.6.

1.5 Experimental Models

To obtain experimental models, system identification was performed on the obtained frequency response data (FRD). The system identification of the substructures, see Sect. 1.4.1, was conducted using an automated method for order selection and identification developed by Yaghoubi and Abrahamsson, see [29, 32]. This method is based on obtaining a number of realisations of the same dataset, using MATLAB's `n4sid` method, which is a state-space subspace method, see McKelvey et al. [28]. The realisations is then statistically evaluated, using the MOC, to discard non-physical modes. The only input required by the user is a high model order from start. In general, the method worked very well for the experimental data of the blade. Only occasionally did it give non-physical modes that could be removed manually. The synthesised models correlate well with measured data and the spread in response between the different blades can be seen in Fig. 1.8.

1.6 Results

In this section correlation between the eigenvalues of the blade models and the blade bracket coupled models are presented. Then, analytical coupling between the components is presented together with the experimental-analytical coupling results. Comparisons between the state-space and the frequency-based methods compared to analytical coupling and finally results based on measurements compared to experimental-analytical coupling.

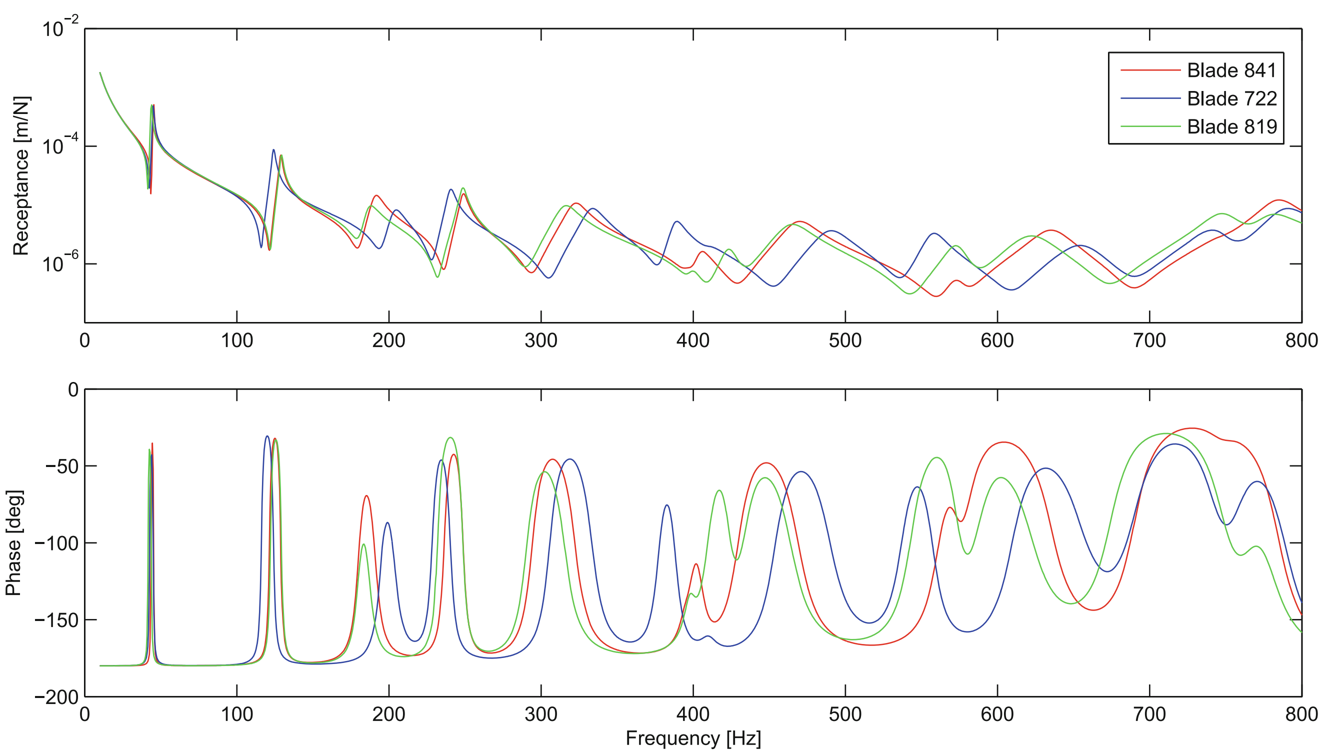

Fig. 1.8 Spread between the synthesised FRFs of the blades with input in z and output from channel 7

Table 1.1 Eigenfrequencies (Hz) and mass (g) for all the blades along with mean (μ, Hz and g), standard deviation (σ, Hz and g) and coefficient of variation (COV, %) of all the experimental blades

	Blades				Statistics			
Component	841	722	819	FEA	μ	σ	COV	$Error$
Mode 1	45.37	45.00	43.72	45.82	44.70	0.86	1.93	2.51
Mode 2	128.76	124.08	129.24	130.67	127.36	2.85	2.24	2.60
Mode 3	190.79	203.49	186.66	197.65	193.65	8.77	4.53	2.06
Mode 4	248.64	240.32	248.44	254.21	245.80	4.75	1.93	3.42
Mode 5	322.12	333.15	315.29	339.93	323.52	9.01	2.79	5.07
Mode 6	395.36	388.16	398.94	412.58	394.16	5.49	1.39	4.67
Mode 7	404.56	410.33	423.24	453.22	412.71	9.56	2.32	9.82
Mode 8	468.74	489.54	463.86	495.47	474.05	13.64	2.88	4.52
Mode 9	572.88	557.26	573.00	598.12	567.71	9.05	1.59	5.36
Mode 10	635.25	654.52	621.72	660.11	637.16	16.49	2.59	3.60
Mode 11	746.52	742.21	747.93	758.33	745.55	2.98	0.40	1.71
Mass	830.50	829.70	830.10	797.11	830.10	0.40	4.89e−04	−3.97

The FE model eigenfrequencies (Hz) and mass (g) are also shown along with the relative error (%) between the measured mean and the FE element blade

Table 1.2 Eigenfrequencies (Hz) for all the bracket mounted blades along with the error (%) between the measured mean and the experimental-analytical synthesised components with the state-space method

Set	Blades/brackets				Error		
Component	μ	SS 841/FEA	SS 722/FEA	SS 819/FEA	Error 1	Error 2	Error 3
Mode 1	40.19	43.01	41.92	41.08	5.39	4.24	3.89
Mode 2	115.73	119.52	114.17	120.55	2.04	2.04	2.03
Mode 3	193.79	187.35	201.35	184.91	−1.11	−1.3	−1.59
Mode 4	222.7	229.24	220.29	229.33	1.54	0.64	2.63
Mode 5	321.03	308.69	322.83	304.88	−3.21	−2.92	−2.15
Mode 6	365.02	391.92	355.8	391.27	6.51	−0.34	5.72
Mode 7	383.58	410.04	405.19	408.84	9.37	4.46	5.38
Mode 8	486.16	437.3	466.13	442.78	−7.93	−8.24	−6.89
Mode 9	536.26	548.52	518.58	537.05	0.51	−1.9	0.49
Mode 10	653.62	584.9	606.98	582.37	−7.75	−13.3	−7.09
Mode 11	726.88	634.01	645.84	617.42	−14.68	−11.58	−12.68

Error 1 stand for the relative error between SS 841/FEA and measured mean, Error 2 between SS 722/FEA and measured mean and Error 3 between SS 819/FEA and measured mean

1.6.1 Analytical and Synthesised Blade Models

The 11 first eigenfrequencies for the three experimental blade models and the FE blade are shown in Table 1.1 along with the mean (μ, Hz), the standard deviation (σ, Hz) and the coefficient of variance (COV, %) for the three experimental blades. Also, the relative error (%) between the measured mean relative to the FE blade is given. It can be seen that the spread between the blades is considerable and that the errors for modes 8 and 10 are considerably larger compared to the other modes. The mass (gramme) is also given in the table for the three blades and the FE blade along with the mean (gramme) of the three blades, the standard deviation (gramme), the coefficient of variance and the relative error with respect to the FE model. It should also be noted that the spread of the mass is very small.

1.6.2 Blade Bracket

From Table 1.2 it can be seen that a relatively large spread is obtained for mode 7, 8, 10 and 11.

In Fig. 1.9 the FRFs for the difference between the coupled models are shown for models coupled using frequency based and state space coupling. It can be seen that the two coupling procedures produces identical results.

In Fig. 1.10 the difference between the individual measured FRFs of the blade bracket assemblies as well as the state space coupled systems becomes eminent.

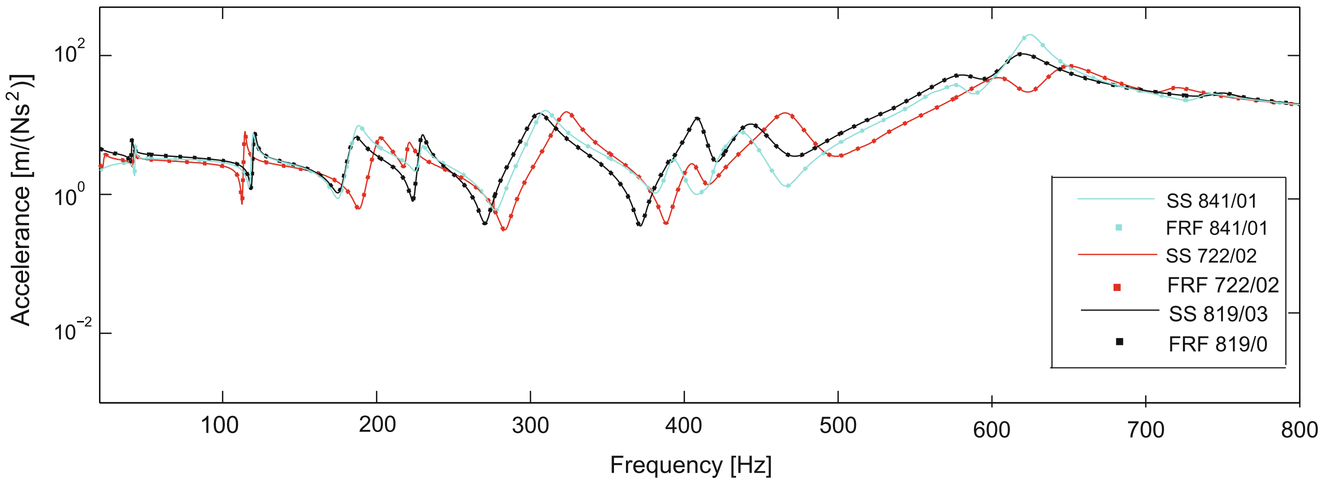

Fig. 1.9 Difference between frequency based and state-space based substructuring methods when **CB = 0**, for experimental-analytical coupling of the blade bracket system

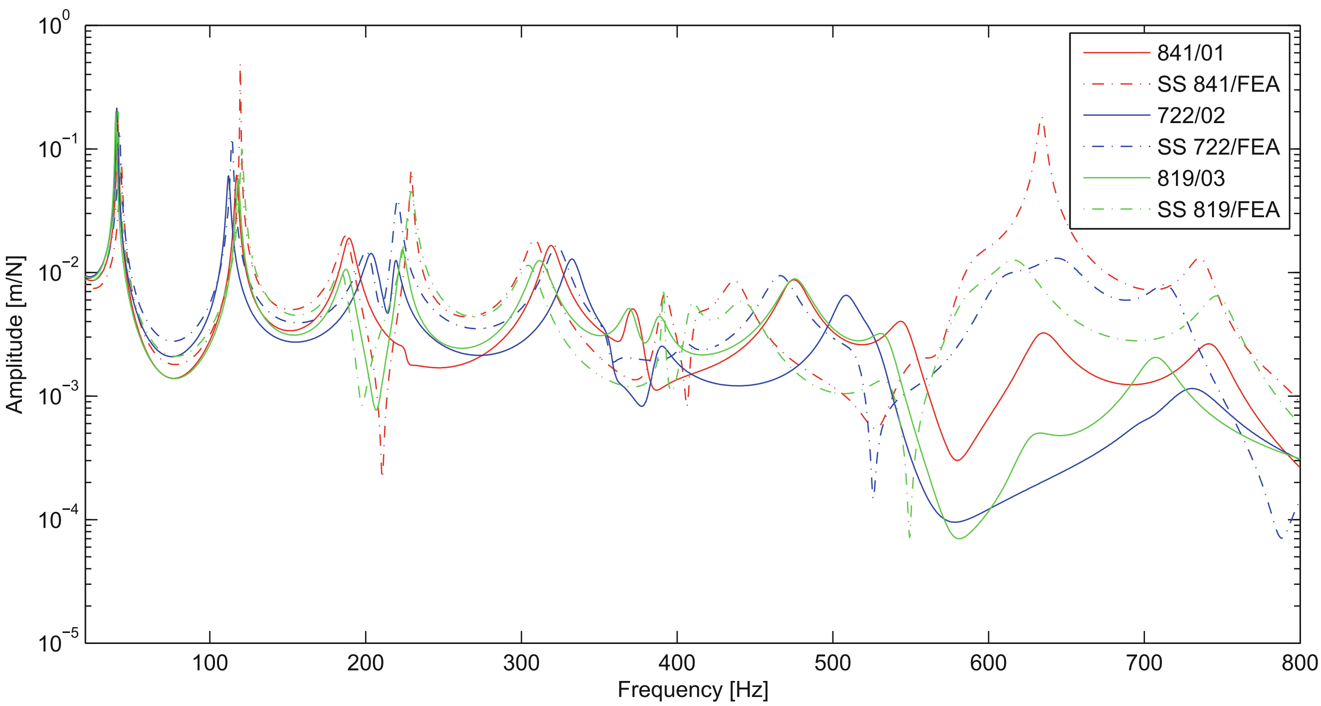

Fig. 1.10 FRF comparison between the coupled state space blade bracket models and the measured models

In Fig. 1.11, the three considered configurations of the analytical couplings are compared to the measured components. The analytical model correlated well with the four first modes. After that the analytical model did not correlate very well with any of the blades.

1.7 Conclusions and Further work

In this paper, an experimental-analytical synthesis of components for the SEM Substructuring focus group test bed, the Ampair 600W wind turbine, has been presented using a state-space method for the coupling. Experimental models of the blades of the turbine were identified through system identification techniques and coupled to analytical models of the brackets

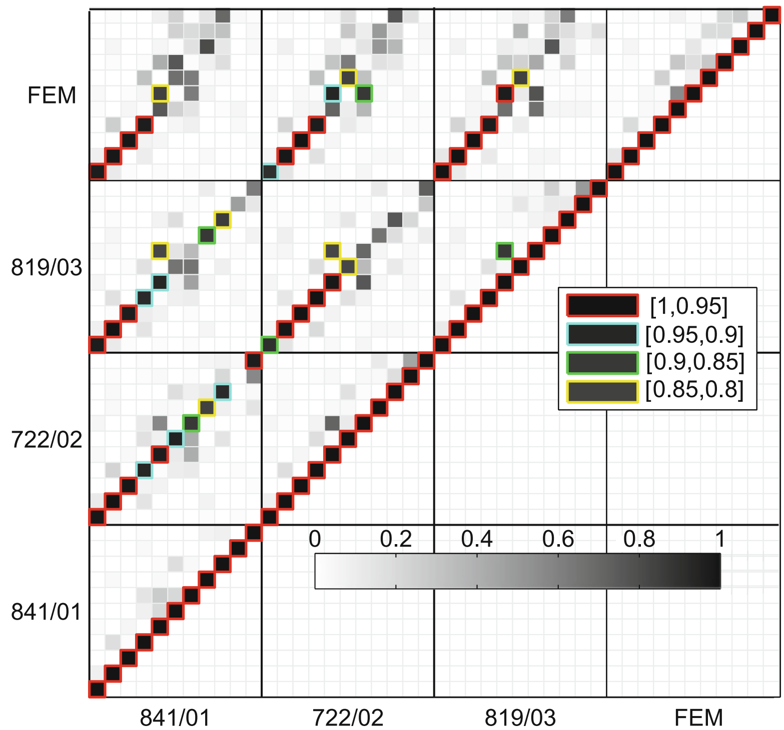

Fig. 1.11 MAC matrix for the 11 first modes between the experimental (measured) models and the three different coupling configurations of the analytical bracket mounted blade. Four colour codes are given where *red* marks a correlation between 0.95 and 1, *cyan* a correlation between 0.9 and 0.95, *green* a correlation between 0.85 and 0.9 and *yellow* a correlation between 0.8 and 0.85 (Color figure online)

normally used to fix them to the hub. The results were compared to those of a frequency-based method and the results were equivalent.

A comparison with results obtained from coupling a finite element blade model to the same bracket model as the experimental models has been performed. When using the same coupling configuration, the experimental-analytical coupling version outperforms the analytical-analytical one. Owing to the greater flexibility in adapting the interface between the two analytical models however, the analytical-analytical model can be tuned to show slightly better results than the experimental ones, see further the full MSc report by Gibanica [5]. This motivates investigation of interfacing techniques such as the transmission simulator method in the context of state-space substructuring.

A theoretical comparison to a second order system coupling technique was performed for the state-space synthesis. It shows that, under certain conditions, the system produced by the method is equal to that obtained by component mode synthesis/direct coupling techniques. The state-space method is also translated into the general framework of de Klerk et al. [1].

An ad-hoc solution for enforcing passivity to systems identified through system identification has been utilized in this paper. In the future, further theoretical development of this technique is needed.

Also, the next step will be to couple the blades together through the hub.

References

1. de Klerk D, Rixen DJ, Voormeeren SN (2008) General framework for dynamic substructuring: history, review and classification of techniques. AIAA J 46(5):1169–1181
2. Bishop RED, Johnson DC (1960) The mechanics of vibration. Cambridge University Press, Cambridge
3. Jetmundsen B, Bielawa RL, Flannelly WG (1988) Generalized frequency domain substructure synthesis. J Am Helicopter Soc 33(1):55–54
4. Craig RR Jr, Bampton MCC (1968) Coupling of substructures for dynamic analyses. AIAA J 6:1313–1319
5. Gibanica M (2013) Experimental-analytical dynamic substructuring: a state-space approach. Master's thesis, Chalmers University of Technology
6. Mayes RL (2012) An introduction to the sem substructures focus group test bed - the ampair 600 wind turbine. In: Conference proceedings of the Society for Experimental Mechanics series. 30th IMAC, a conference on structural dynamics, pp 61–71
7. Mayes RL (2012) Tutorial on experimental dynamic substructuring using the transmission simulator method. In: Conference proceedings of the Society for Experimental Mechanics series. 30th IMAC, a conference on structural dynamics, pp 1–9
8. Rohe DP, Mayes RL (2013) Coupling of a bladed hub to the tower of the ampair 600 wind turbine using the transmission simulator method. In: Conference proceedings of the Society for Experimental Mechanics series. 31th IMAC, a conference on structural dynamics

9. Nurbhai M, Macknelly D (2013) Dynamic substructuring wind turbine blade finite element model update and correlation with test. In: Conference proceedings of the Society for Experimental Mechanics series. 31th IMAC, a conference on structural dynamics
10. Rahimi S, de Klerk D, Rixen DJ (2013) The ampair 600 wind turbine benchmark: results from the frequency based substructuring applied to the rotor assembly. In: Conference proceedings of the Society for Experimental Mechanics series. 31th IMAC, a conference on structural dynamics
11. Brunetti J, Culla A, D'Ambrogio W, Fregolent A (2013) Selection of interface dofs in hub-blade(s) coupling of ampair wind turbine test bed. In: Conference proceedings of the Society for Experimental Mechanics series. 31th IMAC, a conference on structural dynamics
12. SEM Substructuring Focus Group (2013) SEM Substructuring Wiki. http://substructure.engr.wisc.edu/substwiki/. October 2013
13. Steinepreis D, Reuss P, Schempp F, Gaul L (2013) Interface damping of the ampair wind turbine test bed (presentation only). In: Conference proceedings of the Society for Experimental Mechanics series. 31th IMAC, a conference on structural dynamics
14. Sjövall P, Abrahamsson T (2007) Component system identification and state-space model synthesis. Mech Syst Signal Process 21(7): 2697–2714
15. Su T-J, Juang J-N (1994) Substructure system identification and synthesis. J Guid Control Dyn 17(5):1087–1095
16. Harvie J, Avitabile P (2012) Comparison of some wind turbine blade tests in various configurations. In: Conference proceedings of the Society for Experimental Mechanics series. 30th IMAC, a conference on structural dynamics, pp 73–79
17. Nurbhai M, Macknelly D (2012) Modal assessment of wind turbine blade in preparation of experimental substructuring. In: Conference proceedings of the Society for Experimental Mechanics series. 30th IMAC, a conference on structural dynamics, pp 71–72
18. Macknelly D, Nurbhai M, Monk N (2013) Additional modal testing of turbine blades and the application of transmission simulator substructuring methodology for coupling. In: Conference proceedings of the Society for Experimental Mechanics series. 31th IMAC, a conference on structural dynamics
19. Gibanica M, Johansson AT, Rahrovani S, Khorsand M, Abrahamsson T (2013) Spread in modal data obtained from wind turbine blade testing. In: Conference proceedings of the Society for Experimental Mechanics series. 31th IMAC, a conference on structural dynamics
20. Johansson AT, Lindholm C-J, Khorsand M, Abrahamsson T (2013) Modeling and calibration of small-scale wind turbine blade. In: Conference proceedings of the Society for Experimental Mechanics series. 31th IMAC, a conference on structural dynamics
21. Linderholt A (2013) Model calibration of an a600 wind turbine blade. In: Conference proceedings of the Society for Experimental Mechanics series. 31th IMAC, a conference on structural dynamics
22. Antoulas AC (2005) Approximation of large-scale dynamical systems. Advances in design and control. Society for Industrial and Applied Mathematics, Philadelphia
23. Kailath T (1980) Linear systems. Prentice-Hall, Englewood Cliffs
24. Craig RR, Kurdila AJ (2006) Fundamentals of structural dynamics, 2nd edn. Wiley, New York
25. Abrahamsson T (2000) Linear system theory in vibration engineering. Applied Mechanics, Anders Johansson, Chalmers
26. Ewins DJ (2000) Modal testing: theory and practice, 2nd edn. Research Studies Press, Letchworth
27. Ljung L (1999) System identification: theory for the user, 2nd edn. Prentice Hall, Upper Saddle River
28. McKelvey T, AkCay H, Ljung L (1996) Subspace-based multivariable system identification from frequency response data. IEEE Trans Automat Control 41(7):960–979
29. Yaghoubi V, Abrahamsson T (2012) Automated modal analysis based on frequency response function estimates. In: Conference proceedings of the Society for Experimental Mechanics series. 30th IMAC, a conference on structural dynamics, pp 9–18
30. McKelvey T, Moheimani SOR (2005) Estimation of phase constrained mimo transfer functions with application to flexible structures with mixed collocated and non-collocated actuators and sensors. In: Proceedings of the 16th IFAC world congress
31. Sjövall P (2004) Component synthesis and identification in structural dynamics. Licentiate thesis, Chalmers University of Technology
32. Yaghoubi V, Abrahamsson T (2013) The modal observability correlation as a modal correlation metric. In: Conference proceedings of the Society for Experimental Mechanics series. 31th IMAC, a conference on structural dynamics

Chapter 2
Experimental Dynamic Substructuring of the Ampair Wind Turbine Test Bed

Jacopo Brunetti, Antonio Culla, Walter D'Ambrogio, and Annalisa Fregolent

Abstract In a recent paper, the authors discussed the selection of a reduced set of interface DoFs in order to describe the coupling between the blades and the hub of the Ampair test bed wind turbine rotor. The study was conducted using simulated FRFs obtained from Finite Element model of the blades and the hub, but in view of using experimental FRFs. In this paper, test data measured on the turbine by the UW-Madison participants in the IMAC Focus Group on Experimental Dynamic Substructuring, and posted on the Wiki page of the group, are used for dynamic substructuring of the wind turbine test bed.

Keywords Experimental dynamic substructuring • Wind turbine • Modal identification • Frequency response function synthesis • Frequency based substructuring

2.1 Introduction

Experimental Dynamic Substructuring is a very powerful tool in the analysis of dynamic behavior of complex mechanical systems and responds to actual industrial needs. Two main problem can be defined that allow to perform the addition (coupling) and the subtractions (decoupling) of substructures.

In experimental contexts, coupling techniques allow to estimate the dynamic response of a complex structure that cannot be tested in one piece while the model of the component systems can be derived from experimental tests. On the contrary, decoupling techniques can be useful in complete structures where some components cannot be accessed easily or when some components cannot be removed and tested separately.

Addition of substructures (coupling) can be seen as a structural modification problem [1]. Similarly, the decoupling problem can be seen as a structural modification problem with negative modification. Due to modal truncation problems, in experimental dynamic substructuring, the use of FRFs (Frequency Based Substructuring) can be preferred with respect to the use of modal parameters. The main algorithm for frequency based substructuring is the improved impedance coupling [2] that involves just one matrix inversion with respect to the classical impedance coupling technique that requires three inversions. A general framework for dynamic substructuring is provided in [3, 4]: in this context, the so called dual domain decomposition is very useful for experimental application, since it allows to retain the full set of global DoFs by ensuring equilibrium at the interface between substructures. A similar formulation for the decoupling problem is developed and discussed in [5–7].

J. Brunetti
Dipartimento di Ingegneria Industriale e dell'Informazione e di Economia, Università dell'Aquila, Via G. Gronchi, 18
I-67100 L'Aquila (AQ), Italy

LaMCos, Contacts and Structural Mechanics Laboratory, Université de Lyon, CNRS, INSA-Lyon, UMR 5259, rue des Sciences, 69621 Villeurbanne, France

A. Culla • A. Fregolent
Dipartimento di Ingegneria Meccanica e Aerospaziale, Università di Roma La Sapienza, Via Eudossiana 18, I 00184 Rome, Italy

W. D'Ambrogio (✉)
Dipartimento di Ingegneria Industriale e dell'Informazione e di Economia, Università dell'Aquila, Via G. Gronchi, 18
I-67100 L'Aquila (AQ), Italy
e-mail: walter.dambrogio@univaq.it

M. Allen et al. (eds.), *Dynamics of Coupled Structures, Volume 1: Proceedings of the 32nd IMAC, A Conference and Exposition on Structural Dynamics, 2014*, Conference Proceedings of the Society for Experimental Mechanics Series,
DOI 10.1007/978-3-319-04501-6_2, © The Society for Experimental Mechanics, Inc. 2014

In this paper, dynamic substructuring is applied to the Ampair 600 wind turbine. This system has been proposed as a test bed by the Society of Experimental Mechanics focus group on experimental dynamic substructuring, to enable advancements in experimental dynamic substructuring technology and theory. Several specimens of the turbine have been bought by some participants in the focus group. A description of the turbine with modifications made to the system to make it more linear is presented in [8] together with results from a rudimentary modal test on the whole turbine. In a recent paper [9], the authors discussed the selection of a reduced set of interface DoFs in order to describe the coupling between the blades and the hub of the Ampair test bed wind turbine rotor. The study was conducted using simulated FRFs obtained from Finite Element model of the blades and the hub, but in view of using experimental FRFs.

The experimental FRFs used in this paper are measured by UW-Madison on the full turbine, on the two-bladed turbine and on a mass-loaded bladed, and are posted on the Wiki page of the IMAC Experimental Dynamics Substructuring Focus Group. Curve fitting of raw measured FRFs is performed after a reciprocity analysis aimed to select the more convenient reference DoFs, using a poly-reference Least Square Frequency Domain technique. Since some unmeasured FRFs are required to apply the coupling procedure, they are synthesized using the identified modal parameters. Finally, the results of substructuring are presented and discussed.

2.2 Coupling and Decoupling in the Frequency Domain

The coupled structural system is assumed to be made by two (or more) subsystems joined through a number of couplings (see Fig. 2.1). The degrees of freedom (DoFs) of the coupled system can be partitioned into internal DoFs (not belonging to the couplings) and coupling DoFs.

2.2.1 Addition of Subsystems

If addition of subsystems (coupling problem) is considered, all subsystems are assumed to be known whilst the FRF of the coupled system is unknown. In the frequency domain, the equation of motion of a linear time-invariant subsystem r may be written as:

$$\left[Z^{(r)}(\omega)\right]\left\{u^{(r)}(\omega)\right\} = \left\{f^{(r)}(\omega)\right\} + \left\{g^{(r)}(\omega)\right\} \tag{2.1}$$

where:

$[Z^{(r)}]$ is the dynamic stiffness matrix of subsystem r;
$\{u^{(r)}\}$ is the vector of degrees of freedom of subsystem r;
$\{f^{(r)}\}$ is the external force vector;
$\{g^{(r)}\}$ is the vector of connecting forces with other subsystems (constraint forces arising from compatibility conditions).

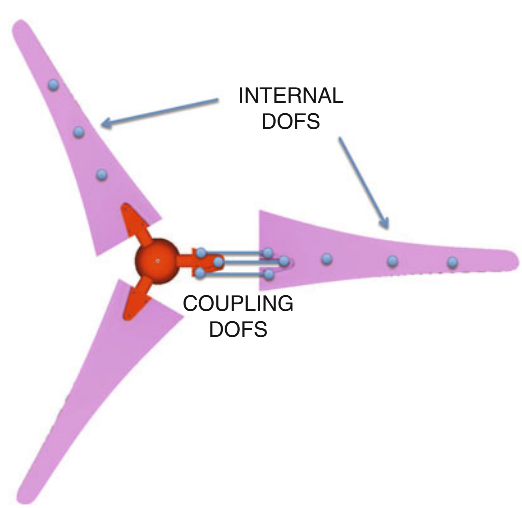

Fig. 2.1 Scheme of the substructuring problem

For the sake of simplicity, the explicit frequency dependence will be omitted. Furthermore, the procedure will be developed with reference to two subsystems, bearing in mind that it can be easily extended to more subsystems.

The equation of motion of the subsystems to be coupled can be written in a block diagonal format as:

$$[Z]\{u\} = \{f\} + \{g\} \quad \text{i.e.} \quad \begin{bmatrix} [Z^{(1)}] & [0] \\ [0] & [Z^{(2)}] \end{bmatrix} \begin{Bmatrix} \{u^{(1)}\} \\ \{u^{(2)}\} \end{Bmatrix} = \begin{Bmatrix} \{f^{(1)}\} \\ \{f^{(2)}\} \end{Bmatrix} + \begin{Bmatrix} \{g^{(1)}\} \\ \{g^{(2)}\} \end{Bmatrix} \tag{2.2}$$

The compatibility condition at the interface DoFs implies that any pair of matching DoFs $u_l^{(1)}$ and $u_m^{(2)}$, i.e. DoF l on subsystem 1 and DoF m on subsystem 2 must have the same displacement, that is $u_l^{(1)} - u_m^{(2)} = 0$.

This condition can be generally expressed as:

$$[B]\{u\} = \{0\} \qquad \text{i.e.} \qquad \begin{bmatrix} [B^{(1)}] & [B^{(2)}] \end{bmatrix} \begin{Bmatrix} \{u^{(1)}\} \\ \{u^{(2)}\} \end{Bmatrix} = 0 \tag{2.3}$$

where each row of $[B]$ corresponds to a pair of matching DoFs. Note that $[B]$ is, in most cases, a signed Boolean matrix and it can be written by distinguishing the contribution of the different subsystems.

The equilibrium condition for constraint forces associated with the compatibility conditions implies that, when the connecting forces are added for a pair of matching DoFs, their sum must be zero, i.e. $g_l^{(1)} + g_m^{(2)} = 0$: this holds for any pair of matching DoFs. Furthermore, if DoF k on subsystem 1 (or 2) is not a connecting DoF, it must be $g_k^{(1)} = 0$: this holds for any non-interface DoF.

Overall, the above conditions can be expressed as:

$$[L]^T \{g\} = \{0\} \tag{2.4}$$

where the matrix $[L]$ is a Boolean localisation matrix. Note that the number of rows of $[L]^T$ is equal to the number of non-interface DoFs plus the number of pairs of interface DoFs.

Equations (2.2)–(2.4) can be put together to obtain the so called 3-field formulation [3]:

$$\begin{cases} [Z]\{u\} = \{f\} + \{g\} \\ [B]\{u\} = \{0\} \\ [L]^T \{g\} = \{0\} \end{cases} \tag{2.5}$$

2.2.1.1 Dual Formulation in the Frequency Domain [3]

In the dual formulation, the total set of DoFs is retained, i.e. each interface DoF is present as many times as there are substructures connected through that DoF. The equilibrium condition $g_l^{(1)} + g_m^{(2)} = 0$ at a pair of interface DoFs is ensured by choosing, for instance, $g_l^{(1)} = -\lambda$ and $g_m^{(2)} = \lambda$. Due to the construction of $[B]$, the overall interface equilibrium can be ensured by writing the connecting forces in the form:

$$\{g\} = -[B]^T \{\lambda\} \tag{2.6}$$

where $\{\lambda\}$ are Lagrange multipliers corresponding to connecting force intensities. Since there is a unique set of connecting force intensities $\boldsymbol{\lambda}$, the interface equilibrium condition Eq. (2.4) is satisfied automatically for any $\boldsymbol{\lambda}$, i.e.

$$[L]^T \{g\} = -[L]^T [B]^T \{\lambda\} = \{0\} \tag{2.7}$$

Then $[B]^T$ is the nullspace of $[L]^T$, so Eq. (2.7) is always satisfied and the system of Eq. (2.5) becomes:

$$\begin{cases} [Z]\{u\} + [B]^T \{\lambda\} = \{f\} \\ [B]\{u\} = \{0\} \end{cases} \tag{2.8}$$

In matrix notation:

$$\begin{bmatrix} [Z] & [B]^T \\ [B] & [0] \end{bmatrix} \begin{Bmatrix} \{u\} \\ \{\lambda\} \end{Bmatrix} = \begin{Bmatrix} \{f\} \\ \{0\} \end{Bmatrix} \tag{2.9}$$

that is:

$$\begin{bmatrix} \left[Z^{(1)}\right] & [0] & \left[B^{(1)}\right]^T \\ [0] & \left[Z^{(2)}\right] & \left[B^{(2)}\right]^T \\ \left[B^{(1)}\right] & \left[B^{(2)}\right] & [0] \end{bmatrix} \begin{Bmatrix} \{u^{(1)}\} \\ \{u^{(2)}\} \\ \{\lambda\} \end{Bmatrix} = \begin{Bmatrix} \{f^{(1)}\} \\ \{f^{(2)}\} \\ \{0\} \end{Bmatrix} \tag{2.10}$$

Note that $[B^{(1)}]$ and $[B^{(2)}]$ extract the coupling DoFs among the full set of DoFs.

By eliminating $\{\lambda\}$, it is possible to obtain a relation in the form $\{u\} = [H]\{f\}$, which provides the FRF of the coupled system [6]:

$$\{u\} = \left([Z]^{-1} - [Z]^{-1}[B]^T\left([B][Z]^{-1}[B]^T\right)^{-1}[B][Z]^{-1}\right)\{f\} \tag{2.11}$$

In expanded notation:

$$\begin{aligned} \begin{Bmatrix} \{u^{(1)}\} \\ \{u^{(2)}\} \end{Bmatrix} = & \left(\begin{bmatrix} \left[Z^{(1)}\right] & [0] \\ [0] & \left[Z^{(2)}\right] \end{bmatrix}^{-1} - \begin{bmatrix} \left[Z^{(1)}\right] & [0] \\ [0] & \left[Z^{(2)}\right] \end{bmatrix}^{-1} \begin{bmatrix} \left[B^{(1)}\right]^T \\ \left[B^{(2)}\right]^T \end{bmatrix} \right. \\ & \times \left(\left[\left[B^{(1)}\right] \left[B^{(2)}\right] \right] \begin{bmatrix} \left[Z^{(1)}\right] & [0] \\ [0] & \left[Z^{(2)}\right] \end{bmatrix}^{-1} \begin{bmatrix} \left[B^{(1)}\right]^T \\ \left[B^{(2)}\right]^T \end{bmatrix} \right)^{-1} \\ & \left. \times \left[\left[B^{(1)}\right] \left[B^{(2)}\right] \right] \begin{bmatrix} \left[Z^{(1)}\right] & [0] \\ [0] & \left[Z^{(2)}\right] \end{bmatrix}^{-1} \right) \begin{Bmatrix} \{f^{(1)}\} \\ \{f^{(2)}\} \end{Bmatrix} \end{aligned} \tag{2.12}$$

i.e., by introducing the FRFs $[H^{(1)}]$ and $[H^{(2)}]$ at the full set of DoFs instead of $[[Z^{(1)}]]^{-1}$ and $[[Z^{(2)}]]^{-1}$:

$$\begin{aligned} \left[H^{RU}\right] = & \begin{bmatrix} \left[H^{(1)}\right] & [0] \\ [0] & \left[H^{(2)}\right] \end{bmatrix} - \begin{bmatrix} \left[H^{(1)}\right] & [0] \\ [0] & \left[H^{(2)}\right] \end{bmatrix} \begin{bmatrix} \left[B^{(1)}\right]^T \\ \left[B^{(2)}\right]^T \end{bmatrix} \\ & \times \left(\left[\left[B^{(1)}\right] \left[B^{(2)}\right] \right] \begin{bmatrix} \left[H^{(1)}\right] & [0] \\ [0] & \left[H^{(2)}\right] \end{bmatrix} \begin{bmatrix} \left[B^{(1)}\right]^T \\ \left[B^{(2)}\right]^T \end{bmatrix} \right)^{-1} \left[\left[B^{(1)}\right] \left[B^{(2)}\right] \right] \begin{bmatrix} \left[H^{(1)}\right] & [0] \\ [0] & \left[H^{(2)}\right] \end{bmatrix} \end{aligned} \tag{2.13}$$

With the dual formulation, the rows and columns corresponding to the coupling DoFs appear twice in $[H^{RU}]$. Obviously, only independent entries are retained.

2.2.2 *Subtraction of Subsystems Using the Dual Domain Decomposition [6]*

If subtraction of subsystems (decoupling problem) is considered, the coupled structural system RU and a residual subsystem R are assumed to be known whilst the FRF of subsystem U is unknown. The unknown subsystem U and the residual subsystem R are joined through a number of couplings (see Fig. 2.2). The degrees of freedom (DoFs) of the coupled system can be partitioned into internal DoFs (u) of subsystem U (not belonging to the couplings), internal DoFs (r) of subsystem R, and coupling DoFs (c).

It is required to find the FRF of the unknown substructure U starting from the FRF of the coupled system RU. The subsystem U can be extracted from the coupled system RU by canceling the dynamic effect of the residual subsystem R. This can be accomplished by adding to the coupled system RU a fictitious subsystem with a dynamic stiffness opposite to that of the residual subsystem R and satisfying compatibility and equilibrium conditions. According to this point of view, the interface between the coupled system RU and the fictitious subsystem should not only include the coupling DoFs between

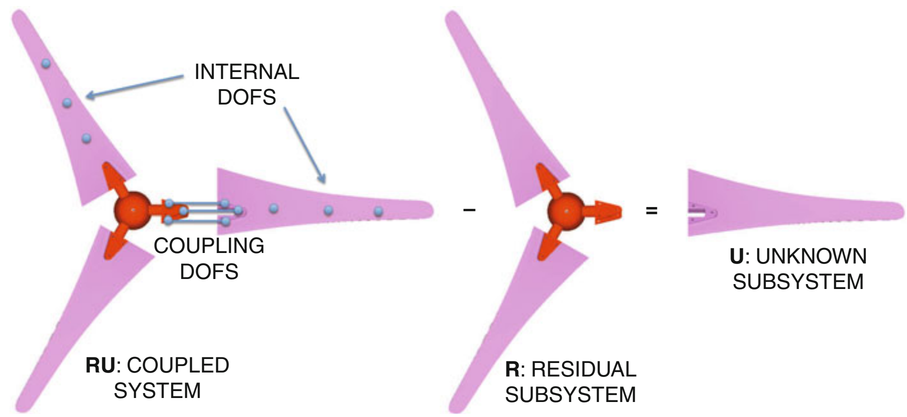

Fig. 2.2 Scheme of the decoupling problem

subsystems U and R, but should as well include the internal DoFs of subsystem R. However, it can be shown that the problem can be solved by considering a number of interface DoFs at least equal to the number of coupling DoFs n_c. Therefore, three options for interface DoFs can be considered:

- standard interface, including only the coupling DoFs (c) between subsystems U and R;
- extended interface, including also some internal DoFs ($i \subseteq r$) of the residual substructure;
- mixed interface, including some coupling DoFs ($d \subseteq c$) and/or some internal DoFs ($i \subseteq r$) of the residual substructure.

In the framework of the dual formulation in the frequency domain (see Sect. 2.2.1.1), the union between the coupled system RU and the fictitious subsystem can be written (see Eq. (2.10)) as:

$$\begin{bmatrix} [Z^{RU}] & [0] & [B_E^{RU}]^T \\ [0] & -[Z^R] & [B_E^R]^T \\ [B_C^{RU}] & [B_C^R] & [0] \end{bmatrix} \begin{Bmatrix} \{u^{RU}\} \\ \{u^R\} \\ \{\lambda\} \end{Bmatrix} = \begin{Bmatrix} \{f^{RU}\} \\ \{f^R\} \\ \{0\} \end{Bmatrix} \tag{2.14}$$

Following the same procedure used in Sect. 2.2.1.1, it is possible to obtain the FRF of the unknown subsystem U.

$$\begin{aligned}[H^U] = &\begin{bmatrix} [H^{RU}] & [0] \\ [0] & -[H^R] \end{bmatrix} - \begin{bmatrix} [H^{RU}] & [0] \\ [0] & -[H^R] \end{bmatrix} \begin{bmatrix} [B_E^{RU}]^T \\ [B_E^R]^T \end{bmatrix} \\ &\times \left(\begin{bmatrix} [B_C^{RU}] & [B_C^R] \end{bmatrix} \begin{bmatrix} [H^{RU}] & [0] \\ [0] & -[H^R] \end{bmatrix} \begin{bmatrix} [B_E^{RU}]^T \\ [B_E^R]^T \end{bmatrix} \right)^{-1} \begin{bmatrix} [B_C^{RU}] & [B_C^R] \end{bmatrix} \begin{bmatrix} [H^{RU}] & [0] \\ [0] & -[H^R] \end{bmatrix} \end{aligned} \tag{2.15}$$

Note that $[H^{RU}]$ and $[H^R]$ are the FRFs at the full set of DoFs of the coupled system and the residual subsystem.

2.3 Test Structure

In this paper the dynamic behavior of the Ampair 600 wind turbine is analyzed. The rotor is composed by three blades clamped to the hub by three bolt and two aluminum plates that sandwich each blade. The rotor is positioned at the top of an aluminum pole fixed on a heavy basement. The whole structure is supported on an elastic trampoline during experimental tests.

Blades are made of glass reinforced polyester and they are coated with a white epoxy. Internal components of the rotor are eliminated and replaced by a dummy mass. The cavity of the hub is filled by a potting material to fix all the components and block the pitch mechanism of the blades.

Non-linearities of composite materials are very hard to model numerically and experimental characterization is the best way to obtain a reliable representation of the dynamic behavior of the blade.

In this paper two substructures are considered to solve the coupling problem. The first subsystem is the blade and the other substructure is the turbine without a blade. Experimental data of the two subsystems are provided by the University of Wisconsin—Madison and can be coupled by means of frequency based substructuring to find the behavior of the whole system.

2.4 Experimental Dynamic Substructuring

In this section the results of experimental dynamic substructuring performed on the Ampair Wind turbine are reported. The dynamic behavior of the whole system is predicted by coupling the mass loaded blade and the two bladed turbine subsystems by means of the Frequency Based Substructuring technique. The predicted FRFs are compared with those measured on the assembled system.

2.4.1 Experimental Data Description

The experimental data used for this substructuring are the data shared by the University of Wisconsin—Madison on the Wiki of the substructuring focus group, acquired on the mass loaded blade and on the two bladed turbine.

Data provided for the mass loaded blade are acceleration FRFs (inertances) measured over three response DoFs by accelerometers placed at two different points (on the tip and on the root of the blade) and for 59 different excitation DoFs, roving the instrumented hammer over 27 points along different directions (Fig. 2.3a). Three nodes are located in correspondence with the three bolts used to fix the blade to the rest of the structure (nodes 16, 17, 18) and excitations are applied on the three spatial directions for each of the three nodes.

A mass-load is applied on the mounting interface of the blade to simulate how the blade is held by the wind turbine. This mass is composed by a block of steel sandwiched between two aluminum plates. This mass results to be rigid in the frequency range of interest. Starting from the pictures published on the wiki internet site, a solid model of the mass is built and inertial characteristics (mass and moments of inertia) are calculated.

The experimental data used to characterize the two-bladed turbine subsystem are measured on three points with bi-axial accelerometers. Excitations are applied by an instrumented hammer over 94 DoFs placed on 51 different points. Also in this case, three nodes are placed in correspondence with the coupling interface and excitations are applied on the nine translational DoFs (Fig. 2.3b).

The dynamic response of the whole turbine is obtained coupling the two subsystems and canceling the load mass effect from the coupled structure.

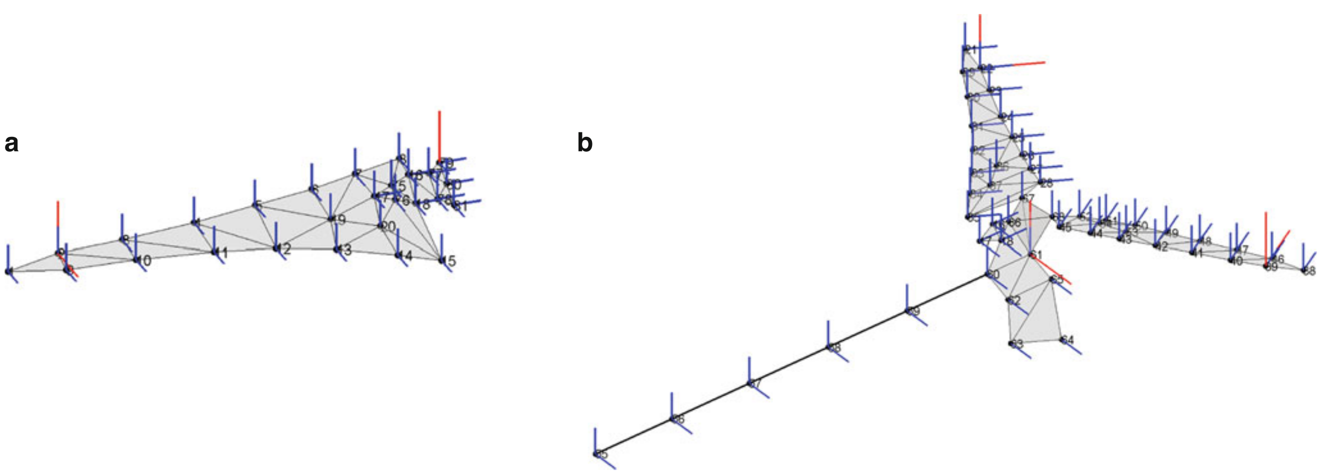

Fig. 2.3 Nodes and directions of the measured data. — excitation DoFs; — response DoFs. (**a**) Measured inertances on the mass loaded blade subsystem. (**b**) Measured inertances on the 2 bladed turbine subsystem (Color figure online)